Engineering Analysis with Boundary Elements 125 (2021) 201–207

Contents lists available at ScienceDirect

Engineering Analysis with Boundary Elements

journal homepage: www.elsevier.com/locate/enganabound

Evaluation of the 4-D singular and near singular potential integrals via the Stokes' theorem

Damir Latypov

BerrieHill Division, Applied Research Associates Inc, 7735 Paragon Road, Dayton, OH, United States

ARTICLE INFO

Keywords:
Boundary element method
Singular and near singular integrals
Electrostatics
Helmholtz kernel

ABSTRACT

A closed-form solution for singular and near-singular double surface integrals arising in boundary integral equations of electrostatics is given for the case of arbitrary coplanar polygonal surfaces. To date, a limited number of closed-form solutions for these integrals were published only for the case of coincident triangular surfaces. The second result of the paper is the evaluation method itself, which is extendable to non-coplanar and non-polygonal surfaces. The main idea of the evaluation method is to construct exact differential forms to perform integration via the Stokes' theorem. Free of coordinates, the differential forms approach has several important advantages over the traditional algebraic singularity subtraction and singularity cancellation methods. Numerical tests on triangles show that the proposed method maintains accuracy even as the aspect ratio of a triangle tends to infinity while the existing methods fail in that limit. Thus, the results of this paper are expected to greatly improve the accuracy and efficiency of the computational electrostatics codes. We also show that the proposed method is extendable to other kernels, e.g., Helmholtz, and therefore has the potential to greatly speed up the matrix build of the computational electromagnetics and acoustics codes.

1. Introduction

Numerical discretization of the boundary integral equations for 3-D problems requires evaluation of the double surface, i.e. 4-D integrals, see Eq. (1). For well separated surfaces, these 4-D integrals can be accurately evaluated via a tensor product of low-order Gaussian quadrature rules. However, when surfaces are coincident, touching (singular case) or close to each other (near-singular case), numerical evaluation of these integrals becomes challenging due to the singularity of a Green's function at $r = r'$. Development of an efficient quadrature rule in this case is exacerbated by two considerations. First, due to proliferation of possible surface shapes encountered in practice, it is highly desirable for the quadrature rule not to be surface shape specific. Second, the total number of quadrature points for the entire 4-D integral can be very large even when only a few quadrature points are required to perform each of the four 1-D integrations – the so-called "curse of dimensionality".

A large body of literature exists on various methods to evaluate integral (1) in a singular and near-singular case. A comprehensive review of this literature is not attempted here. Instead, a set of references is carefully chosen to summarize the lessons learned and to put our work into the context of the known results. The existing methods can be broadly classified as singularity cancellation [2–8] and singularity subtraction [9–11]. The main goal of both methods is to deal with the $1/R$ denominator of a Green's function. They focus on the inner surface integral, often called a source integral, which is singular or nearly singular when the source point $\boldsymbol{r}'$ coincides with or close to the point $\boldsymbol{r}$ of the outer, or test, integral. The singularity subtraction methods tend to be more efficient, i.e., they typically require fewer quadrature points than the singularity cancellation methods to reach a given accuracy level. However, this comes with the requirement to evaluate the $1/R$ source integral as function of $\boldsymbol{r}$ in closed form. This is not convenient in practice due to proliferation of possible surface shapes [4]. For this reason, singularity cancellation techniques have become more popular in recent times. Regardless of the method used to evaluate the source integral, numerical experiments have shown that the remaining test integral is still not amenable to an efficient evaluation by the standard Gaussian quadrature rules [5], especially in the case of coincident surfaces. This means that the integrand of the test integral is not a sufficiently smooth function. Since no clear explanation has yet been given to this fact, we provide one here.

In the case of electrostatic problems, the source integral in (1) is the potential due to a charge distribution χ on the surface S'. As is well-known, the potential is an everywhere continuous function [12]. Its gradient, the electric field, however, must satisfy the boundary conditions when crossing the surface S'. They dictate that the normal to the boundary of S' component of the electric field is discontinuous when crossing in and out of the surface S' [12]. Since the potential is a part of the test integrand, the discontinuity of its derivative explains the slow convergence of the Gaussian quadrature.

E-mail address: dlatypov@ara.com

https://doi.org/10.1016/j.enganabound.2021.01.018
Received 19 October 2020; Received in revised form 25 January 2021; Accepted 26 January 2021
Available online 5 February 2021

To deal with the non-smoothness of the test integrand, in [7,8] a singularity cancellation method has been extended from the 2-D source integral alone to the entire 4-D integral. It has been shown that a rearrangement of integration order can make the integrands of the first three integrals smooth. Numerical testing of the method in [5] demonstrated an improved efficiency over the prior methods and led to a hypothesis that all "*resulting integrands are analytic and, therefore, the integrals can be efficiently approximated by means of simple Gaussian quadrature*". In a later publication [13], the authors however retracted the hypothesis and stated that the method is limited to "*well-shaped (i.e. equilateral) triangular elements pairs*". Such a conclusion is, to a degree, an artefact of a specific implementation of the method. Namely, the method was implemented for triangular surfaces and for uniformity of the implementation, a given triangle was first transformed into a reference equilateral triangle. The smoothness of the Jacobian of such a transformation obviously depends on how close the given triangle is to the one it is being transformed into. Since the Jacobian of the transformation becomes a part of the integrand, one arrives to the quoted conclusion. The method, however, can be implemented without such a transformation, and we have done so [14]. The sharp dependence of the integration accuracy on the closeness of the actual surface to the equilateral triangle then lessened, but the last integration still remained problematic. Given that the integration is a smoothing operation, a situation when the first three integrands are smooth but the last one isn't, may seems counterintuitive. To resolve this puzzle, one must also consider the singularities of the integral (1) as function of the surface shape. For example, in coincident triangular surfaces, it has a logarithmic singularity when the length of one side becomes close to the sum of the remaining two edges, i.e., when the triangle degenerates into a line [9,10]. Since the singularity cancellation method transforms the domain of integration, the singularities associated with the shape of the surfaces propagate into the integrand of the last integral and make its numerical evaluation problematic for degenerate triangles.

In this paper, a novel method to evaluate integral (1) using the Stokes's theorem is proposed. Using this method, the following new results are obtained.

(1) It is shown that the integral (1) can be evaluated in closed form for any pair of polygonal surfaces and arbitrary degree polynomial basis functions. To date, a limited number of closed-form solutions for integral (1) were known only for the case of coincident triangular surfaces [9,10].
(2) In practice, due to the proliferation of possible surface shapes, it is more convenient to evaluate integral (1) using a numerical integration rather than a closed-form solution [5]. Therefore, we also demonstrate a numerical method to evaluate the integral. The method requires evaluation only of 1-D integrals with the integrands which are entire functions, i.e., have the Taylor series with the infinite radius of convergence. As a result, our method produces accurate results even for degenerate surfaces, i.e., triangles with high aspect ratio, (see Fig. 2).
(3) As an example of non-polygonal surface application, a closed-form solution for integral (1) in the case of coincident circular disk surfaces is obtained. Since the circular disk provides the most compact packing of points on a 2-D surface, the result gives the maximum value of the functional $F(S)=\int\int_S dS\int\int_S \frac{1}{R}dS'$ in the class of flat surfaces of unit area.
(4) Finally, it is shown that the 4-D integration method based on the Stokes's theorem can be extended to non-coplanar surfaces and the Green's function of the Helmholtz equation.

The rest of the paper is organized as follows. In Section II, the motivation for using the Stokes's theorem is explained. In Section III, the Stokes's theorem is used to perform two integrations in the 4-D integral, one over the source integral and the second over the test integral. In Section IV, the resulting double contour integral is evaluated in closed form for the case of polygonal surfaces. Section V provides examples and shows how the method can be extended to the cases of non-coplanar surfaces and the Green's function of the Helmholtz equation. Section VI presents conclusions.

2. Problem definition and motivation for the Stokes' theorem

The problem dealt with in this paper is the design of an efficient and accurate algorithm to evaluate the double surface, 4-D integral

$$\int\int_S \varphi(\boldsymbol{r})dS\int\int_{S'} G(\boldsymbol{r},\ \boldsymbol{r}')\chi(\boldsymbol{r}')dS', \tag{1}$$

where $G(\boldsymbol{r}, \boldsymbol{r}')$ is a Green's function, φ and χ are the low order polynomial basis functions [1].

From the discussion of the published results in the Introduction, we deduce the following lessons.

Lesson1: In view of proliferation of possible surface shapes, the algorithm should, as much as possible, be independent of the shape of the surface.

Lesson 2: To avoid the singularity due to non-smoothness of the source (inner) integral of (1), the order of integration in (1) must be rearranged.

Lesson 3: Transformation of the original domain of integration brings singularities associated with the domain's shape into the integrand and thus should be avoided.

Lesson 4: To be efficient, the algorithm must address the curse of dimensionality.

The Stokes' theorem provides a natural way to meet all these requirements. The theorem states that the integral of exterior derivative $d\omega$ of a differential form ω over some orientable manifold Ω is equal to the integral of ω over the boundary of Ω

$$\int_\Omega d\omega=\int_{\partial\Omega}\omega. \tag{2}$$

Differential forms provide an attractive, independent of coordinates approach to multivariate calculus. The Stokes' theorem (2) is invariant with respect to the shape of Ω and the coordinate system used. Since information about the manifold Ω is preserved in $\partial\Omega$, the Stokes' theorem does not bring in the singularities associated with Ω into the integrand ω. Each application of the Stokes' theorem reduces the dimensionality of the integral by 1. Finally, the Stokes' theorem also smoothes the integrand by transforming the exterior derivative $d\omega$ of a differential form ω to the form itself.

In this paper, we demonstrate evaluation of the 4-D integral (1) via the Stokes' theorem in the case of coplanar surfaces and Green's function for the Laplace equation, i.e., electrostatics

$$G(\boldsymbol{r},\ \boldsymbol{r}')=\frac{1}{4\pi|\boldsymbol{r}-\boldsymbol{r}'|}. \tag{3}$$

Choosing the surface plane as the *xy*-plane, integral (1) then can be rewritten as

$$\int\int_S dS\int\int_{S'}\frac{P(x,y,\ x',\ y')}{R}dS',\quad R=\sqrt{(x-\ x')^2+(y-y')^2}, \tag{4}$$

where P is a polynomial function of its arguments.

3. Integrating (4) via the Stokes' theorem

When surfaces S and S' are coplanar, we have the following identity

$$\frac{1}{R}=-\nabla_S\cdot\nabla_{S'}R, \tag{5}$$

where $\nabla_S=\hat{\boldsymbol{x}}\,\partial_x+\ \hat{\boldsymbol{y}}\,\partial_y$ is the differential operator acting on surface S.

Using the Stokes' theorem in the form of the surface gradient theorem [1]

$$\int\int_S \nabla_S f\,dS=\oint_C \hat{\boldsymbol{m}}f\,dl, \tag{6}$$

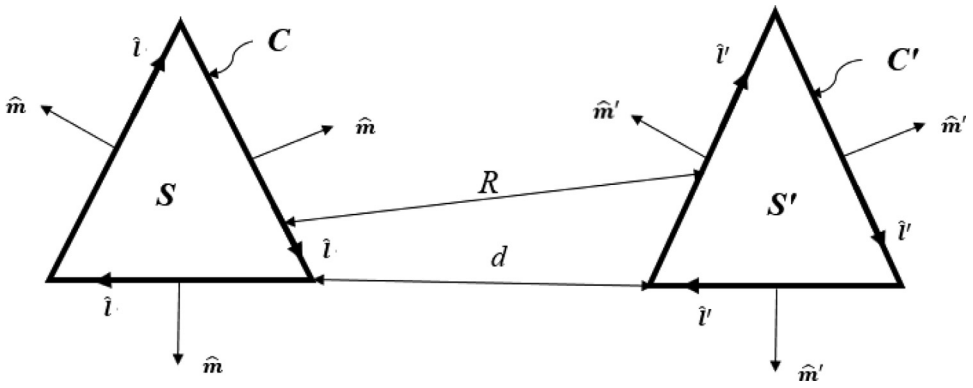

Fig. 1. Geometry illustrating the normal and tangential vectors $\hat{m}$ and $\hat{l}$ to a contour C bounding the surface S, and the distance R between points on the contours C and C' as function of the distance d between the surfaces S and S'.

where C is a closed contour bounding an open surface S, and $\hat{m}$ is the unit vector normal to contour C but tangential to S, and the surface divergence theorem [1]

$$\int\int_S \nabla_S \cdot \boldsymbol{f}\, dS = \oint_C \hat{\boldsymbol{m}} \cdot \boldsymbol{f}\, dl, \tag{7}$$

one can transform the double surface integral of $1/R$ into the double contour integral:

$$\int\int_S dS \int\int_{S'} \frac{1}{R} dS' = -\oint_C \hat{\boldsymbol{m}} dl \cdot \oint_{C'} \hat{\boldsymbol{m}}' R dl' \tag{8}$$

Noting that regardless of the direction in which the contour is traversed

$$\hat{\boldsymbol{m}} \cdot \hat{\boldsymbol{m}}' = \hat{\boldsymbol{l}} \cdot \hat{\boldsymbol{l}}'$$

where $\hat{\boldsymbol{l}}$ and $\hat{\boldsymbol{l}}'$ are the unit vectors tangential to contours C and C', (see Fig. 1). This equation can be written in a more convenient form

$$\int\int_S dS \int\int_{S'} \frac{1}{R} dS' = -\oint_C dl \cdot \oint_{C'} R d\boldsymbol{l}' \tag{9}$$

This is a rather interesting formula. It is valid for any pair of coplanar surfaces S and S'. For example, the utility of this formula for integrating over a circular disk is demonstrated in the Examples section below. Geometrically, Eq. (9) relates the average of the inverse distance between points on a pair of surfaces to the average distance between the points on the directed boundaries of these surfaces. Since the left hand-side of (9) decreases when separation d between the surfaces increases, we must have

$$\lim_{d\to\infty} \oint_C dl \cdot \oint_{C'} R dl' = 0$$

This means cancellation of the leading order in d, $O(d)$ and $O(1)$ terms of the line integrals. Therefore, the double line integral (9) representation may not suitable for numerical evaluation when surfaces are well separated. In this case, however, $1/R$ is a smooth function and direct evaluation of (4) does not present any difficulty.

What about the physical meaning of the right-hand side of (9)? Its resemblance to the formula for a mutual inductance M of two current loops [12]

$$M = \oint_C d\boldsymbol{l} \cdot \oint_{C'} \frac{1}{R} d\boldsymbol{l}' \tag{10}$$

suggests a magnetostatics interpretation. Rewriting R on the left-hand side of (9) as R^2/R, the numerator R^2 could be interpreted as the product of linear currents on the contours C and C' since it is a separable function of the contour parameters. Non-constant currents along the loop, violate the steady-state Kirchhoff's current law, but they do arise in the transient circuits, see e.g., the radiating circuit equation of [15]. Interpretation aside, the formula (9) halves the dimensionality of the integral while smoothing the integrand.

Table 1
Solutions F to (12) for lower order polynomials P.

P	F
1	1
x	$(2x+x')/3$
x^2	$(2R^2+7x^2 + 6xx' + 2\,x'^2)/15$
xx'	$(R^2+3x^2 + 9xx' + 3x'^2)/15$
xy	$(7xy + 3xy' +3x'y + 2x'y')/15$
xy'	$(6xy + 14xy' +4x'y + 6x'y')/30$

To perform integration via the Stokes' theorem for the general case of integral (4) we must find a function F which satisfies

$$\frac{P(\boldsymbol{r},\, \boldsymbol{r}')}{R} = -\nabla_S \cdot \nabla_{S'} \left(R F(\boldsymbol{r},\, \boldsymbol{r}') \right) \tag{11}$$

Let's describe an explicit algorithm to construct representation (11). Performing differentiations in (11) via the chain rule and using (5), gives the following equation

$$-R^2 \nabla_S \cdot \nabla_{S'} F + \boldsymbol{R} \cdot \left(\nabla_S F - \nabla_{S'} F \right) + F = P,\ \ \boldsymbol{R} = \boldsymbol{r} - \boldsymbol{r}' \tag{12}$$

To construct F satisfying this equation, write F as a polynomial of the same degree as P with unknown coefficients. The coefficients are then found by matching term by term of the left and right-hand sides of (12). There are several symmetries one can use to simplify the construction. Since R is symmetric with respect to interchanges $\{x\leftrightarrow x',\ y\leftrightarrow y'\}$ and $\{x\leftrightarrow y,\ x'\leftrightarrow y'\}$, if we know F(x,y,x',y') that satisfies (12) for P(x,y,x',y') then F(y,x,y', x') satisfies (12) for P(y,x,y', x') and F(x',y', x, y) satisfies (12) for P(x',y', x, y). With these symmetries, Table 1 provides F satisfying (12) for any polynomial P up to 2-nd order.

With F satisfying (12), the 4D-integral (4) reduces to the double contour integral

$$\int\int_S dS \int\int_{S'} \frac{P(\boldsymbol{r},\, \boldsymbol{r}')}{R} dS' = -\oint_C d\boldsymbol{l} \cdot \oint_{C'} F\left(r(l), \boldsymbol{r}'(l')\right) R d\boldsymbol{l}' \tag{13}$$

Since F is a polynomial in $\boldsymbol{r}$ and $\boldsymbol{r}'$, it is a linear combination of separable functions of the contour parameters. The coupling of the two contour integrals are thus due to the R and variable angle between the line elements $d\boldsymbol{l}$ and $d\boldsymbol{l}'$.

Eq. (13) is a big step toward efficient evaluation of the original 4-D integral: the dimensionality of the integral has been reduced from 4 to 2, the integrand has been smoothed, and all that happened without surface parametrization and without even specifying its shape. Next, we show that for the important in practice case of polygonal surfaces, the integral (13) can be evaluated in closed-form.

4. Evaluation of double contour integral (13) for coplanar polygonal surfaces

In the important in practice case when surfaces S and S' are polygons, the contours in right hand side of (13) reduce to a set of straight lines,

the angle between $d\boldsymbol{l}$ and $d\boldsymbol{l}'$ is constant, and F turns into a polynomial function of contour parameters

$$F\left(\boldsymbol{r}(l),\boldsymbol{r}'\left(l'\right)\right)=p(l)q\left(l'\right) \tag{14}$$

It is sufficient to evaluate only two types of line integrals

$$J\left(l_1,l_2,\alpha\right)=cos\alpha\int_0^{l_1}p(l)dl\int_0^{l_2}q\left(l'\right)\sqrt{l^2-2ll'\cos\alpha+l'^2}dl' \tag{15}$$

$$J\left(l_1,l_2,h\right)=\int_0^{l_1}p(l)dl\int_0^{l_2}q\left(l'\right)\sqrt{(l'-l)^2+h^2}dl' \tag{16}$$

The first type corresponds to lines originating from the same point and forming angle α and the second corresponds to parallel lines shifted by h. Double line integrals for all other arrangements of two lines on the plane can be constructed from integrals (15) and (16). Details of the evaluation of (15) and (16) are provided in the Appendix. Here we comment on the ideas behind the calculations and important features of the results.

First, the 2-D integrands are turned into separable functions of the variables of integration. The idea is to reduce the problem of a 2D integral evaluation with the complexity $O(n_1n_2)$ to a problem of evaluation of two 1-D integrals with the complexity $O(n_1+n_2)$, where n_1 and n_2 are the number of quadrature points required to evaluate each integral. In the case of integral (15) separability is achieved by a substitution $l'=lt$ and in the case of integral (16) by the substitution $l'=ht+l$. As a result of these substitutions, the inner integral's upper limit becomes dependant on the integration variable of the outer integral, see Eq. (26). If we integrate the resulting expression "as is", the computational complexity of the double line integration would still be $O(n_1n_2)$ since the integrals are coupled through that upper limit of the inner integral. Moreover, the integrand of the last integrals would have a limited smoothness due to a singularity of the type $x^2ln(x)$. By changing of the order of integration, the variable upper integration limit is switched onto the integral with a pure polynomial integrand which can be trivially integrated in closed form. Alternatively, one can get rid of the variable integration limit by another substitution, as shown in the Appendix. The result is given by (28). The final step is to get rid of square root in the integrand. This is done by the standard transformation (29). This transformation is based on the geometrical fact that the arc length of cosh x is equal to the area under the arc:

$$\int_a^b\sqrt{1+\left(\frac{d\cosh(x)}{dx}\right)^2}dx=\int_a^b\cosh(x)dx$$

Let's analyse the result, Eq. (30). Although for brevity of notation we kept writing $q(lt)$ and $p(lt)$, these functions being polynomial are separable in l and t. The limits of integration are constants defined by the geometry of the two lines, their lengths and the angle formed by them. Thus, in (30) we have the product of two independent 1D integrals rather than a 2D integral. The integrands are polynomials in l and the powers of $\sinh(\omega)$ times $\cosh^2(\omega)$ in ω. Thus, both integrands are entire functions (infinitely smooth everywhere on the finite complex plane) which guarantees fast convergence of the Gaussian quadrature. In fact, both integrals allow a closed-form solution since the integral over ω is a table integral [16,17]

$$\int\sinh^n(x)\cosh^2(x)dx$$
$$=\frac{1}{n+1}\sqrt{\cosh^2(x)}\,\mathrm{sech}(x)\sinh^{n+1}(x)\,{}_2^{F_1}\left(-\frac{1}{2},\frac{n+1}{2};\frac{n+3}{2};-\sinh^2(x)\right)$$

We note that in Ref. [18] the coplanar surface case was treated using the divergence theorem. Since the original integrand is scalar, to apply the divergence theorem additional integrations were introduced. As a result, the dimensionality of the integral has not been reduced, i.e., it remained a 4-D integral and no closed-form solution has been obtained.

5. Examples

5.1. Closed-form solution for $\int\int_S dS\int\int_S\frac{1}{R}dS'$ over a circular disk

As a demonstration of the versatility of the method, we compute the integral (4) with $P=1$ when the surface S is coincident with the surface S', and is a circular disk of radius a. Using Eq. (9), the integral is equal to

$$-a^2\int_0^{2\pi}\hat{\boldsymbol{\varphi}}d\varphi\cdot\int_0^{2\pi}\hat{\boldsymbol{\varphi}}'\,Rd\varphi'$$

where we used the fact that for a circle $d\boldsymbol{l}=a\hat{\boldsymbol{\varphi}}d\varphi$. Noting that

$$\hat{\boldsymbol{\varphi}}\cdot\hat{\boldsymbol{\varphi}}'=\cos\left(\varphi'-\varphi\right),\ R=a\sqrt{(\cos\varphi'-cos\varphi)^2+(\sin\varphi'-\sin\varphi)^2}$$

and

$$\int_0^{2\pi}d\varphi\int_0^{2\pi}\cos\left(\varphi'-\varphi\right)\sqrt{1-\cos\left(\varphi'-\varphi\right)}d\varphi'=-8\pi\frac{\sqrt{2}}{3}$$

one finds

$$\int\int_S dS\int\int_S\frac{1}{R}dS'=\frac{16}{3}\pi a^3 \tag{17}$$

Dividing (17) by the area A of the disk squared, we find the average inverse distance between the points on the disk:

$$\frac{1}{R}_{disk}=\frac{16}{3\sqrt{\pi A}}. \tag{18}$$

Since a circular disk provides the most compact arrangement of the points on a plane, the right-hand side of (18) gives the maximum value of the functional F

$$F(S)=\frac{1}{A^2}\int\int_S dS\int\int_S\frac{1}{R}dS'. \tag{19}$$

For comparison, using formula in Ref. [10], one can compute that the value of functional (19) for equilateral triangle is 1.04 times smaller

$$\frac{1}{R}_{equilateral\ triangle}=3^{1/4}\frac{2ln3}{\sqrt{A}} \tag{20}$$

Electrostatic interpretation of this result is that a uniform surface charge density distributed over a circular disk has 4% larger potential energy than the same surface charge uniformly distributed over an equilateral triangle of the same area.

5.2. Numerical results

In this example, performance of the proposed method is compared with the current state-of-the art method of Ref. [5]. Numerical comparison of dissimilar methods is often not an uneasy task. The comparison metric in the case of integration methods can include the number of quadrature points, run times to achieve a given accuracy, etc. These metrics are not absolute. Run times are likely to be implementation dependant. The number of quadrature points required to achieve a given accuracy may not tell the full story either since the methods could end up with integrands of different computational complexity. Therefore, a relative metric has been chosen which shows the rate of accuracy degradation at a fixed number of quadrature points as the surface becomes more degenerate.

In the numerical tests, integral (4) with $P=1$ was computed for coincident isosceles triangles with various values of the aspect ratio. The aspect ratio is defined as

$$AR=\frac{l_1l_2l_3}{8\left(s-l_1\right)\left(s-l_2\right)\left(s-l_3\right)},\qquad s=\frac{1}{2}\left(l_1+l_2+l_3\right)$$

Aspect ratio of 1 corresponds to an equilateral triangle. For base comparison the number of quadrature points was fixed to be the same for the current method as for each of the 8 sub-integrals in the method of Ref. [5]. For an asymptotic behaviour comparison, the accuracy plot

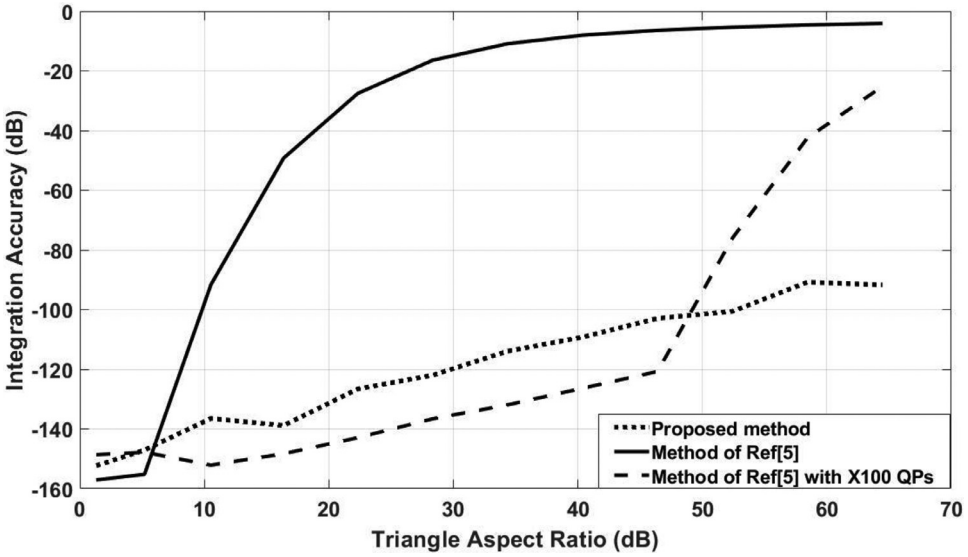

Fig. 2. Integration accuracy with a fixed number of quadrature points as function of triangle aspect ratio.

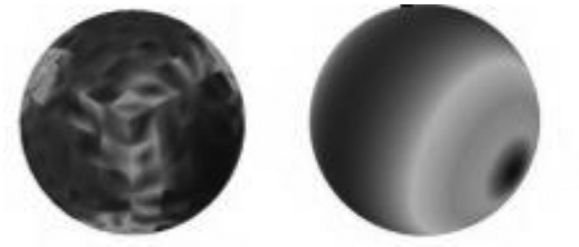

Fig. 3. Impact of the integration accuracy on the onset of the low frequency breakdown for a perfect electric conductor (PEC) sphere with the radius $\lambda/100$. (Left) Solution with low integration accuracy results in visibly wrong, non-smooth, surface current distribution. (Right) solution with accurate integration.

for the method of Ref. [5] was also recomputed with 100 times more quadrature points than in the base comparison. The accuracy was computed in decibels as $10log_{10}|\frac{v-v_{truth}}{v_{truth}}|$, where v is the value of the integral computed using a numerical method and v_{truth} is the ground truth provided by the analytical solution for integral (4) for coincident triangles of Ref. [10]. Fig. 2 shows the results. They confirm the statement from [13] quoted in the Introduction that the method of Ref [5] fails for degenerate triangles. At the same time, the accuracy of the current method (at fixed number of quadrature points) degrades slowly as the triangle degenerates into a line.

Our next example is concerned with the impact of the integration accuracy on the overall solution of the boundary integral equation. A direct way to assess it is to compare numerical solutions obtained at different levels of integration accuracy with the analytical solution. Few problems, however, allow analytical solution. In case of the Electric Field Integral Equation (EFIE) [1], impact of the integration accuracy on the solution can be readily demonstrated using the so called low-frequency breakdown effect. The term "breakdown" refers to a phenomenon whereby as the wavelength of an electromagnetic wave becomes much larger than the size of a scatterer (low frequency), the condition number of the discretized EFIE matrix begins to grow unboundedly. As the result, numerical solution becomes unstable [20]. The onset of this instability at a fixed ratio of the scatterer linear size l to the wavelength λ depends on the integration accuracy. The higher is the accuracy of the integration, the smaller is the ratio l/λ at which the numerical solution breaks down, see Fig. 3.

5.3. Exact differential forms for other kernels

Here we provide the exact differential forms for integrating (4) with $P = 1$ for the case of surfaces on parallel planes, and surfaces on orthogonal planes, as well as the differential forms to integrate

$$\int\int_S dS \int\int_{S'} \frac{e^{-ikR}}{R} dS' \quad \text{and} \quad \int\int_S dS \int\int_{S'} \frac{1}{R^2} dS'$$

for the coplanar surfaces.

1 Surfaces on parallel planes shifted by $z_0 > 0$, $1/R$ kernel

$$\frac{1}{R} = \nabla_S \cdot \nabla_{S'} \big(-R + z_0 ln\big(R + z_0\big)\big), \quad R = \sqrt{(x - x')^2 + (y - y')^2 + z_0^2} \tag{21}$$

2 Surfaces on orthogonal planes, $1/R$ kernel

$$\frac{1}{R} = \nabla_{xz} \nabla_{x'y'} \left\{-R + \big(x' - x\big) ln\big(R + x - x'\big)\right\}, \quad R = \sqrt{(x' - x)^2 + y'^2 + z^2} \tag{22}$$

3 Coplanar surfaces, Helmholtz kernel

$$\frac{e^{-ikR}}{R} = -\nabla_S \cdot \nabla_{S'} \frac{j}{k} Ei(-jkR), \; R = \sqrt{(x - x')^2 + (y - y')^2} \tag{23}$$

where $Ei(x)$ is the exponential integral.

1 Coplanar surfaces, $1/R^2$ kernel

$$\frac{1}{R^2} = -\nabla_S \cdot \nabla_{S'} \left(\frac{1}{2} ln^2 R\right), \quad R = \sqrt{(x - x')^2 + (y - y')^2} \tag{24}$$

These solutions are readily obtained by seeking the required differential forms F as functions of R only, i.e., $F(R)$. This is possible when $P = 1$ since the kernels depend only on R. Using the chain rule, we find

$$\nabla_S \cdot \nabla_{S'} F(R) = F''(R) \nabla_S R \cdot \nabla_{S'} R + F'(R)$$

In the case of coplanar surfaces and the Helmholtz kernel, for example, the resulting differential equation for F is

$$F''(R) + \frac{1}{R} F'(R) = \frac{e^{-ikR}}{R} \tag{25}$$

where we used the fact that for the coplanar surfaces

$$\nabla_S R \cdot \nabla_{S'} R = -\frac{\boldsymbol{R}}{R} \cdot \frac{\boldsymbol{R}}{R} = -1, \quad \nabla_S \cdot \nabla_{S'} R = \nabla_S \cdot \left(-\frac{\boldsymbol{R}}{R}\right) = -\frac{1}{R}$$

The general solution to (25) is $\frac{j}{k} Ei(-jkR) + C_1 \log(R) + C_2$, where $Ei(x)$ is the exponential integral, and C_1 and C_2 are arbitrary constants.

Since we are free to chose any particular solution to (25), we set the these two constants to zero and arrive at the result stated above. Methods to construct the differential forms when $P \neq 1$ will be described in subsequent papers.

6. Conclusion

Efficient and accurate evaluation of singular and near-singular integrals is one of the main remaining problems of the boundary element method. The current state of the art for the singular case has been reviewed in the Introduction. The case of near-singular integrals has been studied much less. The existing methods of dealing with them are ad-hoc in nature and lack mathematical rigour [19]. In this paper, we propose a novel method of integration based on construction of the exact differential forms. The method addresses both, the singular and near-singular integrals and does so in a unified manner. In this paper, the integrals over the coplanar surfaces with the Green's function for the Laplace equation are considered in detail. A closed-form solution is obtained for arbitrary polygonal surfaces, coinciding or not. This is a novel and general result. To date, a limited number of closed-form solutions were known only for the case of coincident triangular surfaces. In practice, it is more convenient to have a numerical method instead of closed-form solutions due to the proliferation of possible surface shapes, their relative positions, etc. Such a numerical method is also demonstrated in this paper. As compared to the current state of the art, it requires far fewer quadrature points and does not fail when the surfaces become degenerate, e.g. in case of the triangles with high aspect ratio. In our next paper, we plan to demonstrate the solution for the integrals over the surfaces on parallel planes, a case which is very important in practice.

Declaration of Competing Interest

There are no conflicts of interest to disclose.

Acknowledgments

The author would like to thank Dr. Tri Van, the Head of the Computational Electromagnetics Group of ARA for support, and Dr. Gregory Wilson for valuable discussions. The author also thanks the anonymous reviewers who helped to make the paper much better.

Appendix A: Double Line Integrals

In this Appendix, we provide the calculations of the double line integrals. The evaluation techniques are well-known, and partial results can be found elsewhere. They are included here for the purpose of completeness.

A.1. Lines forming an angle

A substitution $l'=lt$ transforms integral (15) into

$$J\left(l_1,l_2,\alpha\right) = cos\alpha \int_0^{l_1} p(l)l^2 dl \int_0^{l_2/l} q(lt)\sqrt{1-2t\cos\alpha+t^2}dt \tag{26}$$

The 2-D domain of integration can be decomposed into a rectangle and a hyperbola:

$$\int_0^{l_1} \dots dl \int_0^{l_2/l} \dots dt = \int_0^{l_1} \dots dl \int_0^{l_2/l_1} \dots dt + \int_0^{l_1} \dots dl \int_{l_2/l_1}^{l_2/l} \dots dt \tag{27}$$

By changing the order of integration in the second 2-D integral, we can write

$$\int_0^{l_1} p(l)l^2 dl \int_{l_2/l_1}^{l_2/l} q(lt)\sqrt{1-2tcos\alpha+t^2}dt = \int_{l_2/l_1}^{\infty} \sqrt{1-2tcos\alpha+t^2}dt \int_0^{l_2/t} q(lt)p(l)l^2 dl$$

Next, a substitution $t = 1/z$ leads to

$$\int_{l_2/l_1}^{\infty} \sqrt{1-2tcos\alpha+t^2}dt \int_0^{l_2/t} q(lt)p(l)l^2 dl = \int_0^{l_1/l_2} \sqrt{1-\frac{2}{z}cos\alpha+\frac{1}{z^2}}\frac{dz}{z^2} \int_0^{l_2 z} q(l/z)p(l)l^2 dl$$

Substitution $l = z\tau$ eliminates the dependence of the upper limit of integration on z and results in

$$\int_0^{l_1/l_2} \sqrt{1-\frac{2}{z}cos\alpha+\frac{1}{z^2}}\frac{dz}{z^2} \int_0^{l_2 z} q(l/z)p(l)l^2 dl = \int_0^{l_1/l_2} \sqrt{z^2-2zcos\alpha+1}dz \int_0^{l_2} q(\tau)p(z\tau)\tau^2 d\tau$$

Since the domain of integration is now a rectangle, the order of integration can be changed without affecting the integrand. Combining the two integrals, we find

$$J\left(l_1,l_2,\alpha\right) = cos\alpha\left\{\int_0^{l_1} p(l)l^2 dl \int_0^{\frac{l_2}{l_1}} q(lt)\sqrt{1-2tcos\alpha+t^2}dt + \int_0^{l_2} q(l)l^2 dl \int_0^{\frac{l_1}{l_2}} p(lt)\sqrt{1-2tcos\alpha+t^2}\,dt\right\} \tag{28}$$

The final step is the substitution:

$t = \cos\alpha + \sin\alpha \sinh\omega$

(29) which makes the integrand an entire function of both arguments

$$J\left(l_1,l_2,\alpha\right) = \cos\alpha\sin\alpha|\sin\alpha|\left\{\int_0^{l_1} p(l)l^2 dl \int_{-\operatorname{asinh}(\cot\alpha)}^{\operatorname{asinh}\left(\frac{\frac{l_2}{l_1}-\cos\alpha}{\sin\alpha}\right)} q(lt)\cosh^2\omega d\omega + \int_0^{l_2} q(l)l^2 dl \int_{-\operatorname{asinh}(\cot\alpha)}^{\operatorname{asinh}\left(\frac{\frac{l_1}{l_2}-\cos\alpha}{\sin\alpha}\right)} p(lt)\cosh^2\omega d\omega\right\} \tag{30}$$

A.2. Parallel Lines

$$J\left(l_1,l_2,h\right) = \int_0^{l_1} p(l)dl \int_0^{l_2} q\left(l'\right)\sqrt{(l'-l)^2+h^2}dl' \tag{31}$$

First note, that when $h = 0$

$$J\left(l_1,l_2,0\right) = \int_0^{l_1} p(l)dl\left[\int_0^{l} q\left(l'\right)\left(l-l'\right)dl' + \int_l^{l_2} q\left(l'\right)\left(l'-l\right)dl'\right],$$

and the integral is computable in closed form since all integrands are polynomials. Therefore, we now assume that $h \neq 0$. Making a substitution $l' = l + hu$ and changing the order of integration, one finds

$$J\left(l_1,l_2,h\right) = h^2\left\{\int_{-\frac{l_1}{h}}^{\frac{l_2-l_1}{h}} \sqrt{1+u^2}du \int_0^{l_1} q(l+hu)p(l)dl\right.$$

$$+\int_0^{\frac{l_1}{h}}\sqrt{1+u^2}du\int_0^{hu}q(l-hu)p(l)dl + \int_{\frac{l_2-l_1}{h}}^{\frac{l_2}{h}}\sqrt{1+u^2}du\int_0^{l_2-hu}q(l+hu)p(l)dl\Bigg\} \quad (32)$$

The integrals over l have polynomial integrands and are therefore computed analytically. Their dependence on u is also polynomial. In the outer integrals, the substitution $u = \sinh\omega$ gets rid of the square root and results in the integrand, which is a product of powers of the hyperbolic functions sinh and cosh, i.e., an entire function. Thus, it can be efficiently evaluated using the Gaussian quadrature. A closed-form solution can also be obtained using integral tables [16,17].

References

[1] Jin J. The finite element method in electromagnetics. Wiley; 2002.
[2] Duffy MG. Quadrature over a pyramid or a cube of integrands with a singularity at a vertex. SIAM J Numer Anal 1982;19:1260–2.
[3] Graglia RD. Static and dynamic potential integrals for linearly varying source distributions in two- and three-dimensional problems. IEEE Trans Antennas Propag 1987;35:662–9.
[4] Khayat MA, Wilton DR. Numerical evaluation of singular and near singular potential integrals. IEEE Trans Antennas Propag 2005;53:3180–90.
[5] Polimeridis AG, Vipiana F, Mosig JR, Wilton DR. DIRECTFN: fully numerical algorithms for high precision computation of singular integrals in Galerkin SIE methods. IEEE Trans Antennas Propag 2013;61:3112–22.
[6] Vipiana F, Wilton DR. Numerical evaluation via singularity cancellation schemes of near-singular integrals involving the gradient of Helmholtz-type potentials. IEEE Trans. Antennas Propag 2013;61:1255–65.
[7] Gray LJ, Glaeser JM, Kaplan T. Direct evaluation of hypersingular Galerkin surface integrals. SIAM J. Sci. Comp. 2004;25:1534–56.
[8] Gray LJ, Salvadori A, Phan A-V, Mantic V. Direct evaluation of hypersingular Galerkin surface integrals. II. Electron J Boud Elem 2006;4:105–30.
[9] Eibert TF, Hansen V. On the calculation of potential integrals for linear source distributions on triangular domains. IEEE Trans Antennas Propag 1995;43:1499–502.
[10] Sievers D, Eibert TF, Hansen V. Correction to on the calculation of potential integrals for linear source distributions on triangular domains. IEEE Trans Antennas Prop 2005;53:3113–33.
[11] Järvenpää S, Taskinen M, Ylä-Oijala P. Singularity extraction technique for integral equation methods with higher order basis functions on plane triangles and tetrahedra. Int J Numer Meth Eng 2003;58:1149–65.
[12] Jackson JD. Classical electrodynamics. Wiley; 1975.
[13] Rivero J, Vipiana F, Wilton DR, Johnson WA. Evaluation of 4-D reaction integrals via double application of the divergence theorem. IEEE Trans Antennas Propag 2019;67:1131–42.
[14] D. Latypov, "DIRECTFN method without transformation to an equilateral triangle",Dayton: Internal ARA Report (2020).
[15] Latypov D, Bulmer J. Radiation and near field in resistance-inductor circuit transients. J Appl Phys 2012;111:1–8.
[16] Gradshteyn IS, Ryzhik IM. Table of integrals, series, and products. Elsevier; 2015.
[17] Wolfram Alpha LLC. 2009. https://www.wolframalpha.com/input/?i=integrate+sinh%5En%28x%29*cosh%5E2%28x%29 (access December 22, 2020)
[18] Wilton DR, Vipiana F, Johnson WA. Evaluation of 4-D reaction integrals in the method of moments: coplanar element case. IEEE Trans Antennas Propag 2017;65:2479–93.
[19] Vipiana F, Wilton DR. Numerical evaluation via singularity cancellation schemes of near-singular integrals involving the gradient of Helmholtz-type potentials. IEEE Trans Antennas Propag 2013;61:1255–65.
[20] Mittra R. Computational electromagnetics Editor. Springer; 2014.